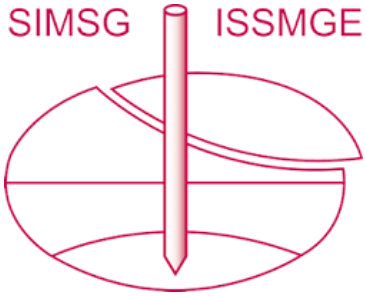
INTERNATIONAL SOCIETY FOR
SOIL MECHANICS AND
GEOTECHNICAL ENGINEERING



This paper was downloaded from the Online Library of the International Society for Soil Mechanics and Geotechnical Engineering (ISSMGE). The library is available here:

https://www.issmge.org/publications/online-library

This is an open-access database that archives thousands of papers published under the Auspices of the ISSMGE and maintained by the Innovation and Development Committee of ISSMGE.

The paper was published in the proceedings of the 6th International Conference on Geotechnical and Geophysical Site Characterization and was edited by Tamás Huszák, András Mahler and Edina Koch. The conference was originally scheduled to be held in Budapest, Hungary in 2020, but due to the COVID-19 pandemic, it was held online from September 26th to September 29th 2021.

Coupled Eulerian-Lagrangian 3D finite-element technique for analysis of dilatometer test in clay

V. Silvestri
École Polytechnique, Montréal, Québec, Canada, vincenzo.silvestri@polymtl.ca

G. Abou-Samra
Université de Moncton, Moncton, Nouveau Brunswick, Canada, ghassan.abou-samra@umoncton.ca

ABSTRACT: A field investigation was carried out in a clay deposit of eastern Canada by means of self-boring pressuremeter tests (SBPM), Marchetti dilatometer tests (DMT), and vane shear tests (VST). Values of undrained shear strength S_u and secant shear modulus G_{sec} obtained from DMTs and VSTs were much lower than SBMTs-deduced values. As vane blades cause partial destructuration of cemented clays, whereas SBPMTs induce only minimal damage, it was believed that DMTs also induced partial breakdown of the clay structures. To gain better insight of the deformations generated during penetration of the dilatometer, the paper presents finite-element analyses (FEA) conducted for the simulation of the continuous deep penetration process (DPP) during the performance of a DMT. The clay is characterized by a linearly elastic perfectly plastic constitutive relationship with strength parameters corresponding to partially destructured clay. Simulations were performed using the Coupled Eulerian-Lagrangian (CEL) finite-element technique integrated in Abaqus/Explicit software to account for excessive soil deformations exhibited during the DPP. Curves of computed contact pressure ($p_{o\text{-}num}$) on the surface of the dilatometer blade as function of penetration depth (d) were determined continuously during the DPP.

Keywords: explicit finite element method; coupled Eulerian-Lagrangian approach; large deformations; dilatometer test; comparisons.

1. Interpretation theory of Marchetti's DMT

The flat dilatometer test (DMT) was introduced by Marchetti [1] as a new in-situ soil penetration test. The equipment and test procedure are simple. The test provides repeatable and nearly continuous data that have been correlated to various soil parameters. A DMT test is performed by pushing the blade of the dilatometer vertically and at a constant rate of 2 cm/s into a soil deposit. The blade is stopped at the depth where the test is to be performed, by first measuring the lift-off pressure and then by inflating the flexible membrane so that the center of the circular membrane reaches 1.1 mm of displacement. In the original development, Marchetti [1] combined the corrected lift-off pressure p_o and the inflation pressure p_1 with the in-situ pore pressure u_o and effective overburden pressure σ'_{vo}, and obtained the following parameters:

$$I_D = \text{Material Index} = (p_1 - p_o) / (p_o - u_o) \quad (1)$$

$$K_D = \text{Lateral stress index} = (p_o - u_o) / \sigma'_{vo} \quad (2)$$

$$E_D = \text{Dilatometer modulus} = 34.7\ (p_1 - p_o) \quad (3)$$

In clays the Lateral stress index, K_D, is of paramount importance, because it is employed for the estimation of: a) the in-situ coefficient of lateral earth pressure, K_o, from the expression

$$K_o = (K_D / \beta_k)^{0.47} - 0.6 \quad (4)$$

with $\beta_k = 1.5$, b) the overconsolidation ratio, OCR, on the basis of

$$OCR = (0.5\ K_D)^{1.56} \quad (5)$$

and c) the undrained shear strength, S_u, using the SHANSEP procedure relating the stress ratio S_u / σ'_{vo} to OCR, that is

$$S_u / \sigma'_{vo} = 0.22\ (0.5\ K_D)^{1.25} \quad (6)$$

The latter expression applies to clays that are either normally consolidated or have been rendered overconsolidated by unloading, but are neither cemented nor sensitive [2].

Because the problem of a rational interpretation of the DMT in clays is still not fully understood, DMT results have often been correlated to limit pressures deduced from conventional pressuremeter tests (PMT), self-boring pressuremeter tests (SBPMT), full-displacement cone pressuremeter tests (FDCPMT), and tip resistances measured in cone penetration tests (CPT), as reported, for example, by [3-7]. But, as the interpretation of pressuremeter tests in undrained clay is amenable to theoretical analysis, whereas that of CPT tests is mostly based on empirical correlations, with the exception of a limited number of studies [8-10], DMT-SBPMT relationships have been favoured by several investigators (see, for example, [5, 11-15]).

However, because the strain distribution that arises around an expanding cylindrical cavity is quite different from that generated during the penetration of the flat blade of the dilatometer, as illustrated by the work of Whittle et al. [16], it was therefore decided to first perform realistic finite element analyses of the

installation phase of the flat dilatometer. A future analysis will simulate the subsequent expansion phase of the dilatometer membrane.

The present paper summarizes finite element analyses carried out based upon constitutive parameters that were obtained from a geotechnical investigation performed in sensitive clay of eastern Canada. Finite element analyses (FEA) were conducted using the software Abaqus/Explicit [17] which integrates a Coupled Eulerian–Lagrangian (CEL) approach; this is in order to compute the contact pressure ($p_{o\text{-}num}$) applied on the circular membrane. The pressure $p_{o\text{-}num}$ is also computed as function of penetration depth (d).

Numerical results are compared to experimental measurements determined by means of DMTs. In addition, clay strength properties retained in the present investigation correspond to post-peak or secant values obtained from self-boring pressuremeter and vane shear tests.

2. 3D CEL FEA of DMT installation: Modeling and numerical results

2.1. Geometry, dimensions and meshing of assembled parts

The 3D blade of the flat dilatometer is assumed to be a rigid part. The blade is 95mm-wide, 220mm-high and 15mm-thick. The lower tapered section of the blade tip is 50mm-long. The blade is made of high strength stainless-steel and therefore is modeled as a rigid body. The membrane has a diameter of 60 mm and is located on the blade vertical face, as shown in Fig. 1.

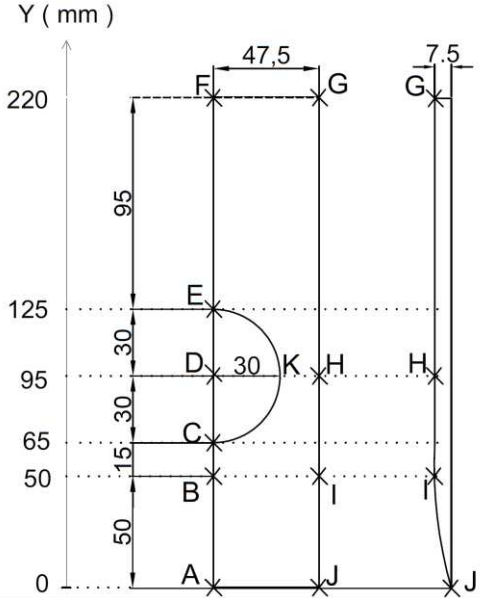


Figure 1. Front and side views of the modeled blade.

The soil is assumed to be a 3D Eulerian part and is modeled as a parallelepiped having a height of 600 cm and a horizontal section of 20 cm x 51 cm. Lateral boundaries of the soil were determined after several trials to ensure that they are far enough from the blade so that the effect of the blade penetration is negligible on these boundaries.

Both parts are symmetrical around perpendicular planes XY and ZY, where Y is the vertical axis and X and Z are the horizontal axes. Consequently, a quarter of the blade and of the soil is used to model the deep penetration process (DPP). The assembly of these parts at the initial state (e.g., corresponding to the undeformed configuration at time $t = 0\ s$) is shown in Fig. 2. The clay medium is meshed with 132835 linear elements (e.g., 156156 nodes) of type EC3D8R which is an Eulerian continuum with 8-noded linear multi-material brick elements with reduced integration and hourglass control. For a better discretization, dimensions of clay elements in close interaction with the blade were chosen very small (e.g., 2.5 mm x 5.0 mm x 7.0 mm).

The dimensions and the Eulerian mesh are also depicted in Figs. 2 and 3. The uppermost half meter of the continuum is modeled material-free at the initial state ($t = 0\ s$). This free-material zone is intended to receive the flowing clay material during blade penetration. This mesh which is composed of 209088 linear elements (e.g., 237875 nodes) of type EC3D8R was also used for the clay.

The blade was discretized using 341 elements (and 768 nodes) of type C3D8R which is integrated in Abaqus/explicit; it is a 8-node linear brick, with reduced integration and hourglass control.

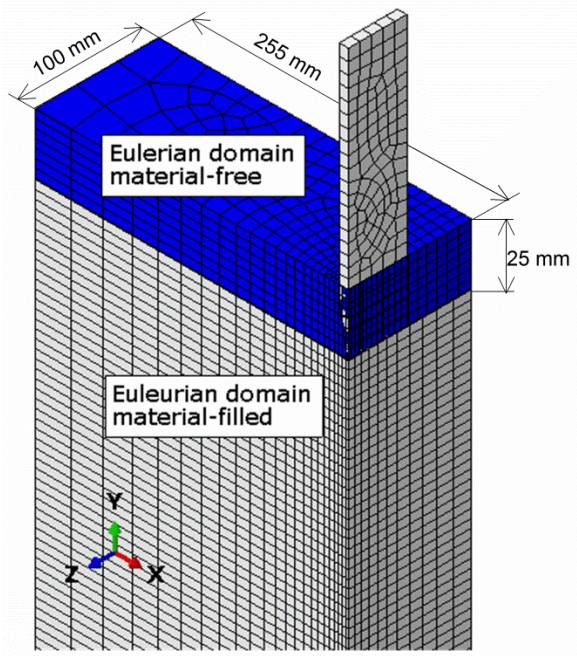


Figure 2. Assembly of the meshed blade and soil within the Eulerian mesh. Undeformed configuration corresponding to the initial state.

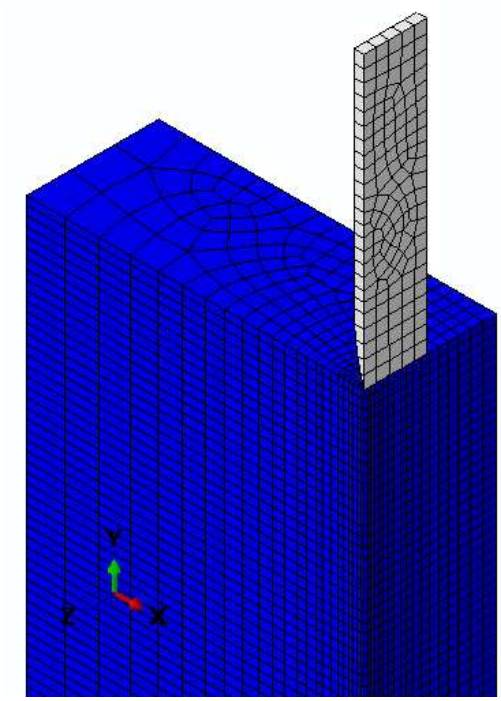


Figure 3. Assembly of the meshed blade and soil-field within the Eulerian mesh. Undeformed configuration corresponding to the initial state.

2.2. Undrained mechanical parameters of clay deposit

The properties of the modeled soil are taken from Silvestri [18]. Dilatometers tests were performed by Hamouche [19] at an experimental site located in the town of Louiseville (Quebec), in eastern Canada, where a 1.8-m thick crust of fissured clay overlies a 60-m thick deposit of sensitive clay. In the depth of study, from 1.8 to 14m, the moisture content decreases from 90 to 65%, the liquidity index ranges from 1.6 to 1.1, and the plasticity index stays constant at 45%. The undrained shear strength, measured with a Nilcon vane, increases linearly with depth, from 20 kPa at 1.8m to 55kPa at 14m. The overconsolidation ratio OCR deduced from oedometer tests decreases from 5.6 at 1.8m to 2.4 at 14m.

Tables 1 and 2 report SBPMT and VST results for the depths where DMTs were performed. Values of shear modulus were obtained from stress-strain curves deduced from the expansion curves of the self-boring pressuremeter tests. The maximum Rigidity index G_{max} / S_u shown in Table 1 is based upon the tangent value of the shear modulus at the origin, whereas the secant value G_{sec} / S_u is based upon the value of the shear modulus deduced at the point where the shear stress on the stress-strain curves equals the undrained shear strength. In addition, the secant Rigidity index reported in Table 2 is equal to the secant shear modulus shown in Table 1 divided by the undrained shear strength obtained from vane shear tests. Furthermore, while the parameter σ_{ho} reported in Table 1 is the deduced at rest horizontal pressure, the parameter σ_{vo} reported in Table 2 equals the computed value of the in situ vertical pressure.

Table 1. Results of SBPMTs

Depth (m)	σ_{h0} (kPa)	S_u (kPa)	G_{max}/S_u	G_{sec}/S_u
3.05	56	36	167	62
4.5	98	48	78	29
6.00	111	49	118	44
Average			121	45

Table 2. Results of VSTs

Depth (m)	σ_{v0} (kPa)	S_u (kPa	G^*_{sec}/S_u
3.05	45	29	77
4.5	68	32	43
6.00	90	35	60
Average			60
* G_{sec} obtained from SBPMTs			

In the present study, it has been assumed that the clay behaves as a linearly elastic perfectly plastic material obeying the von Mises yield criterion. The moving blade displaces the clay which in turn undergoes deformations with no volume change or consolidation. Consequently, the Coupled Eulerian-Lagrangian (CEL) analysis uses an undrained secant Young's modulus (E_u) and a shear strength (S_u). Both E_u and S_u increase linearly with depth in the following manner: $E_u = 2989.69\ kPa$ and $S_u = 23.13\ kPa$ on the ground surface and $E_u = 11350.15\ kPa$ and $S_u = 52.69\ kPa$ at the depth (d) of 14m. The secant value was retained for Young's modulus, because it was believed that the clay medium experienced severe deformations during the installation phase of the dilatometer. Due to conservation of volume in undrained shearing, Poisson's ratio was given a constant value of 0.49 instead of the theoretical value of 0.5; this is simply to avoid numerical singularities.

2.3. Blade-soil interaction

In the CEL analysis, the general contact algorithm integrated in Abaqus/Explicit was used to enforce contact between the surface of the Eulerian material (e.g., the clay) and the Lagrangian surface of the blade. The Eulerian-Lagrangian contact is enforced only for the Lagrangian surface defined on the blade which was considered as a rigid solid. The formulation of contact between soil and blade uses a kinematic contact formulation based on a pure master/slave approach. In this FEA the underformable lateral surface of the rigid blade is the master surface and the slave surface is formed from nodes of elements used for meshing the deformable soil. In this pure master/slave algorithm, the nodes of the master surface can, in principle, penetrate the slave surface but slave nodes cannot penetrate master segments. The finite-sliding formulation integrated in the general contact algorithm is used by Abaqus/Explicit to model the soil-blade interaction. This formulation allows for arbitrary separation, sliding, and rotation of the surfaces in contact. In this paper, it was assumed that the

surface of the blade is smooth and consequentely a frictionless formulation was used to describe the soil-blade interaction.

2.4. Boundary conditions and applied velocity

At the initial state (e.g., for $t = 0\ s$), the tip of the blade is above the ground surface (Fig. 2). The blade installation is then achieved in three successive steps using a dynamic explicit procedure in which the blade is pushed continuously at a vertical and uniform downward penetration velocity (V_{pe}) of 20 cm/s. A zero flow velocity was described normal to the two planes of symmetry (YX and YZ). Also, a zero vertical flow was described normal to the base. Obviously the clay is free to flow into the Eulerian mesh on the top of the model at the initial position of the ground surface; this is a natural condition.

2.5. Effect of blade penetration rate

The velocity retained in the simulation of the blade installation process is 20 cm/s which is ten times larger than the real velocity of 2 $\mathrm{cm/s}$ used when performing a conventional DMT. Because of very small-time increments used in an automatic time incrementation, the runtime should be minimized somehow to get a solution in a reasonable time period. For computational efficiency in the cases of quasi-static analyses such as this study, Abaqus/explicit offers two strategies, e.g., mass scaling and velocity increase. Here, the term quasi-static analysis means accelerating the penetration rate without introducing any significant inertia effects. This acceleration process is always used when dealing with quasi-static analyses performed by using explicit dynamic procedures. Examples of this strategy may be found in: i) Tho et al. [20] who showed that a velocity of 0.3344 m/s was an acceptable rate for the analysis of jack-up spudcan foundations, and ii) Qiu et al. [21] who found that a velocity of 0.5 m/s was slow enough for the analyses of geotechnical problems with large deformations. These authors among many others used a CEL technique based on explicit dynamic procedures. Generally it can be concluded that values of p_{0-num} and penetration force increase with penetration rate. However, in this study, the rate of 20 cm/s was judged adequate to minimize any inertia effects and was selected for the numerical analysis of DPP.

3. FEA results

3.1. Penetration force and bearing capacity coefficient

The output processor allowed determination of several variables of interest. The history of penetration force was determined as function of depth (d) for 20 cm/s rate of penetration. The result is depicted in Fig. 4. The computed curve presents a steep slope for small penetration depths (let's say up to 0.23m, at the beginning of the DPP). This means that a relatively high penetration force is exerted at the start of the DPP. Below the depth of 0.23m, the curve flattens considerably and its slope decreases, so that less vertical force is needed to penetrate the soil at constant velocity. Please recall that as only a quarter of the model was considered, the total vertical penetration force applied on the whole blade equals four times the penetration force reported in Fig. 4. Because of frictionless contact formulation, the penetration force is equivalent to the total vertical force due to the contact pressure acting on the horizontal projection of the tip surface. Tip penetration resistances, q_v, were computed based upon the results of Fig. 4. The following values were obtained: 360.35 kPa at 3.05 m, 424.91 kPa at 4.57 m, and 462.10 kPa at 5.79 m.

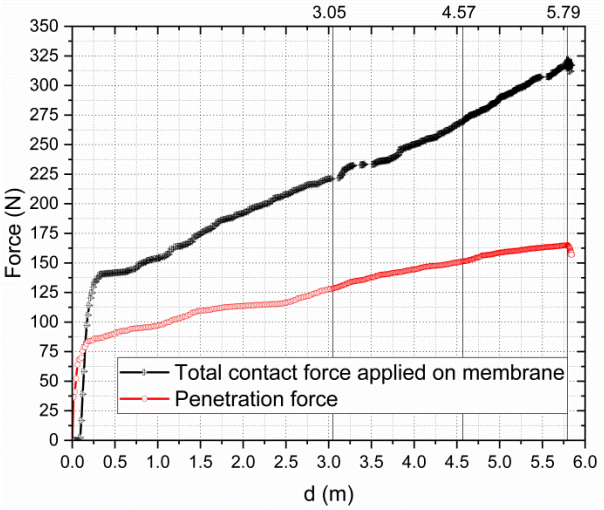


Figure 4. Penetration force versus penetration depth for penetration velocity of 20 cm/s.

By assuming perfect plasticity,these tip resistances enable the determination of the bearing capacity coefficient from the well-known equation, $N_{cv} = (q_v - \sigma_{vo})/S_u$, where σ_{vo} is the in situ total vertical pressure; its value ranges between 10.7 and 10.9 in the depth interval from 3.05 m to 5 79 m, as reported in Fig.5.

The total horizontal force applied on the membrane versus penetration depth is also reported in Fig. 4. This force which is found to be greater than the penetration force allows the determination of the averace contact pressure on the membrane, as discussed next in the paper.

Let p_{0-num} and σ_{ho} denote respectively the computed horizontal contact pressure applied on the membrane and the at rest total horizontal pressure at the same depth d. The parameter N_{ch} which is defined as $N_{ch} = (p_{0-num} - \sigma_{h_o})/S_u$ is also depicted in Fig. 5, where its value is practically constant at 3.8.

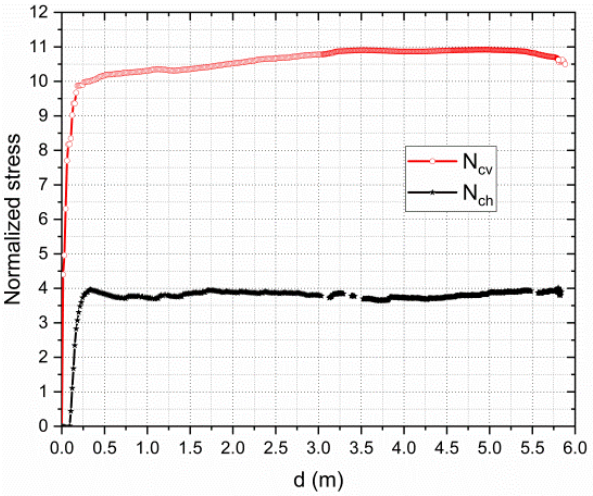


Figure 5. $N_{cv} = (q_v - \sigma_{vo})/S_u$ and $N_{ch} = (p_{0-num} - \sigma_{h_o})/S_u$ versus d for penetration velocity of 20 cm/s.

3.2. Computed contact pressures on membrane compared to experimentally measured lift-off pressures

The computed horizontal contact pressure applied on the membrane (p_{0-num}) versus penetration depth (d) is depicted in Fig. 6.

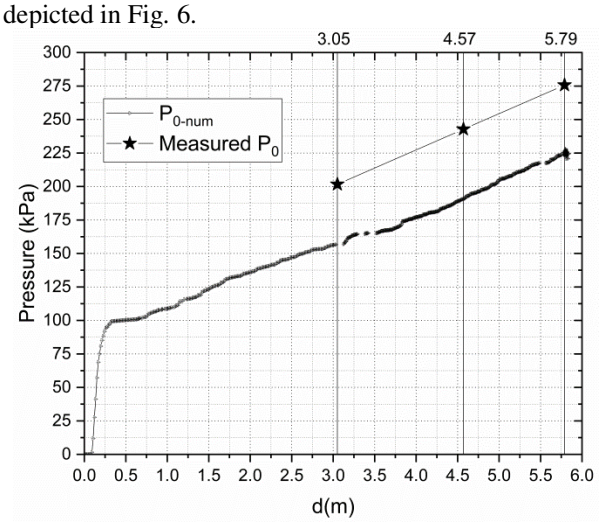


Figure 6. p_{0-num} and measured lift-off pressure p_o versus penetration depth. Curves corresponding to 20 cm/s.

DMTs were completed at the following depths: 3.05 m, 4.57 m, and 5.79 m. While the corresponding values of the initial in situ horizontal pressure, σ_{ho}, were equal to 56 kPa, 98 kPa, and 111 kPa, as reported in Table 1, the measured values of p_o were 201.6 kPa, 242.8 kPa, and 275.70 kPa, as shown in Fig. 6 and Table 3, respectively. For the aforementioned depths, the computed mean contact pressures p_{0-num} were found to be equal to 157.40 kPa, 190.65 kPa, and 223.90 kPa, respectively. These average contact pressures are based upon the computed distribution of nodal contact pressures.The computed values as well as the complete p_{0-num}-d curve are presented in Fig. 6 and in Table 3. The horizontal and vertical drop lines in Fig. 6 correspond to the experimental values determined by Hamouche [19].

Table 3. Results of DMTs and expansion tests

Depth, d (m)	p_0 (kPa) [19]	p_{0-num} (kPa) (computed in this study)	P^*_{lim} (kPa) [22]	P^{**}_{lim} (kPa) [22]
3.05	201.6	157.40	211	200
4.57	242.8	190.65	250	260
5.79	275.70	223.90	289	300
* Obtained from field SBPMTs				
** Obtained from $P_{lim} = \sigma_{ho} + S_u(1 + ln(G_{sec}/S_u))$				

Comparison between the average contact pressures computed on the area of the 60-mm membrane and the experimental values indicates quite conclusively that the finite element analysis fails to adequately represent the observed response. It should be recalled that, as mentioned at the beginning of the present investigation, it was believed that the penetration of the dilatometer blade caused severe destructuration of the cemented clay, as advocated by several investigators (see, for example, Lutenegger [5]). This prompted the writers to adopt constitutive parameters which correspond to a partially destructured material, such as secant Young`s moduli and vane shear strengths. The experimental results thus show that the initial phase of a DMT does not cause partial destructuration of the sensitive clay. This implies that higher values of deformation moduli should be used in order to obtain more realistic contact pressures, as is the case for cylindrical and spherical elastic-plastic expansions. An upcoming investigation will address such point.

This notwithstanding, an attempt was made to find out whether a simple expression based upon the limiting expansion of a cylindrical cavity in an ideally elastic perfectly plastic medium could lead to reasonable estimates of the lift-off pressure, p_o. By using the well-known relationship, $p_{lim} = \sigma_{ho} + Su\ (1+ln\ G_{sec}/S_u)$, the following results are obtained [22]: 211 kPa at 3.05m, 250 kPa at 4.57m, and 289 kPa at 5.79m, based upon the deduced at rest horizontal pressure reported in Table 1 ant the strength parameters indicated in Table 2. Although such values compare well to the measured lift-off pressures reported in Table 3, additional investigations are needed to confirm that such good agreement is not merely coincidental, but also exists in other sensitive clay. The last column in Table 3 also presents the maximum pressures reached in the self-boring pressuremeter tests.

3.3. Stresses, strains and displacements

Contours of equivalent plastic strain at integration points for shallow and deep penetration depths are presented in Fig. 7 and Fig. 8, respectively. These figures show that the equivalent plastic strains are very small, with the exceptions of values computed close to the blade lateral surfaces and tip.The reason for the small values of the plastic strains is partially attributed to assumed frictionless contact beteen the blade and the surrounding clay.

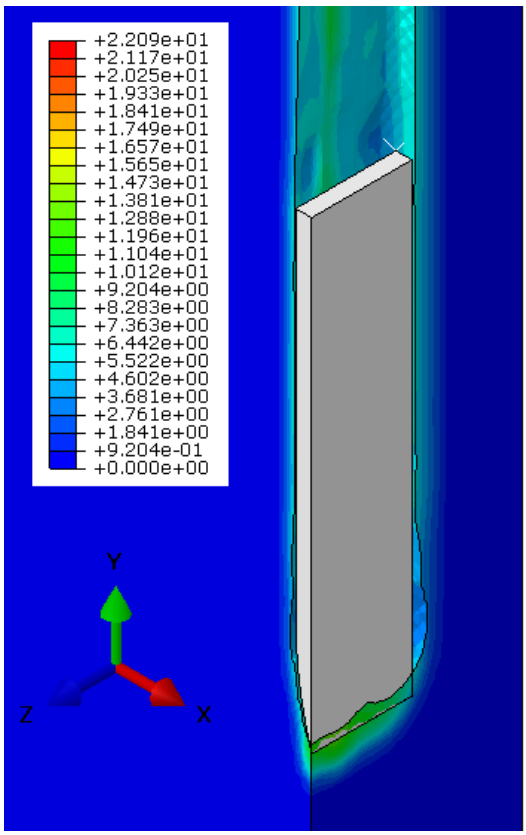


Figure 7. Contours of equivalent plastic strain at integration points for a depth of penetration of 2.61 m.

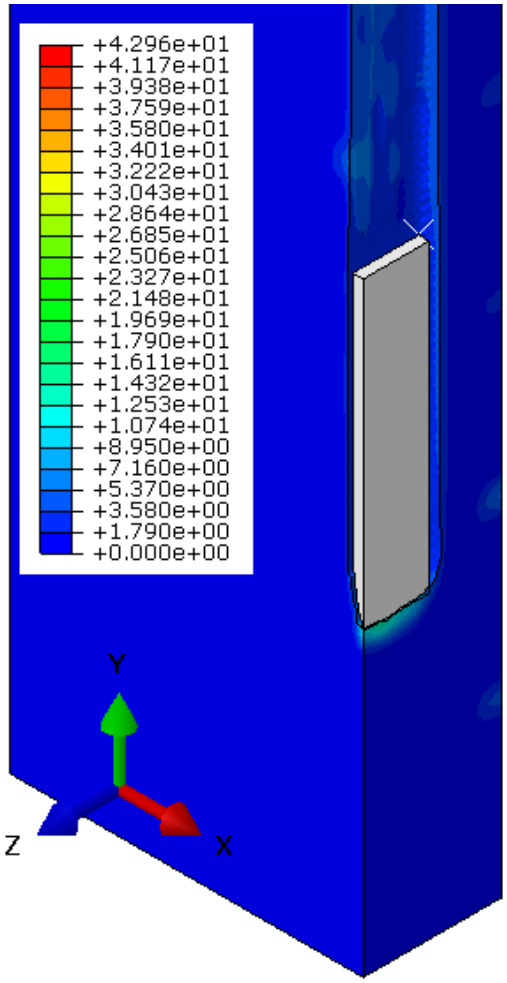


Figure 8. Contours of equivalent plastic strain at a penetration depth of 5.79 m.

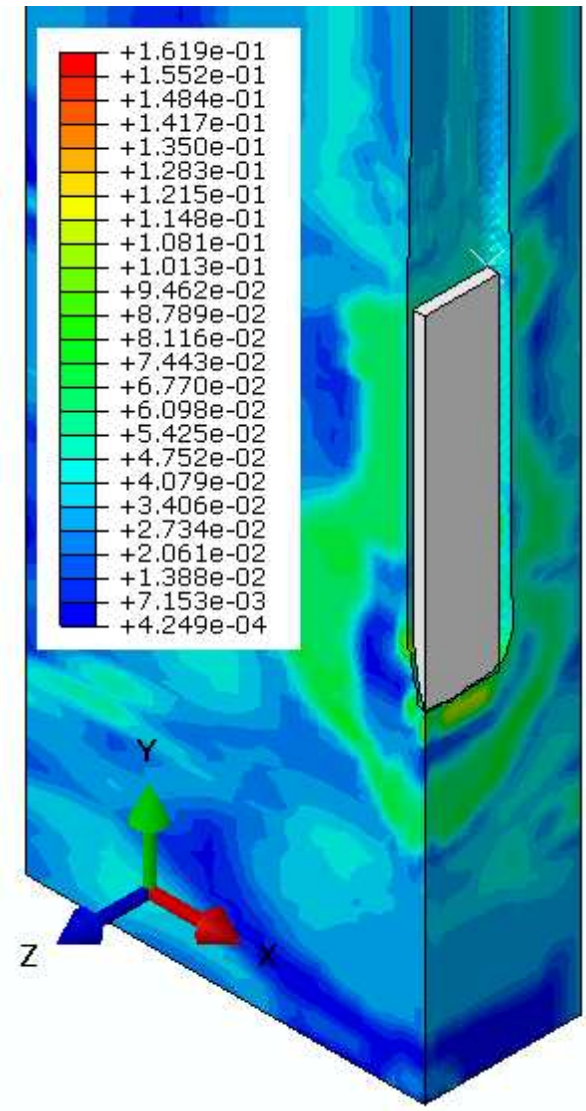


Figure 9. Contours of Mises equivalent stress (in MPa) at a penetration depth of 5.79 m.

Fig. 9 shows contours of Mises equivalent stress at a depth of 5.79 m. The stresses are rather low, even in the vicinity of the dilatometer blade. The reason is again attributed to the low values of Young`s modulus retained in the present study.

While Fig. 10 presents contours of vertical displacements, Fig. 11 shows contours of Mises equivalent stress at a depth of 4.489 m. The vertical displacements in Fig, 10 are negative because of the downward penetration. Again, due to the frictionless interface, the displacements induced in the clay are very small compared to that experienced by the dilatometer. The contours of the Mises equivalent stress reported in Fig. 11 also show that the values which are quite small in the central area of the blade increase slightly as one approaches the top, bottom, and lateral vertical edges of the blade. Please note that the value of the undrained shear strength equals 32 kPa at 4.5 m. as reported in Table 2.

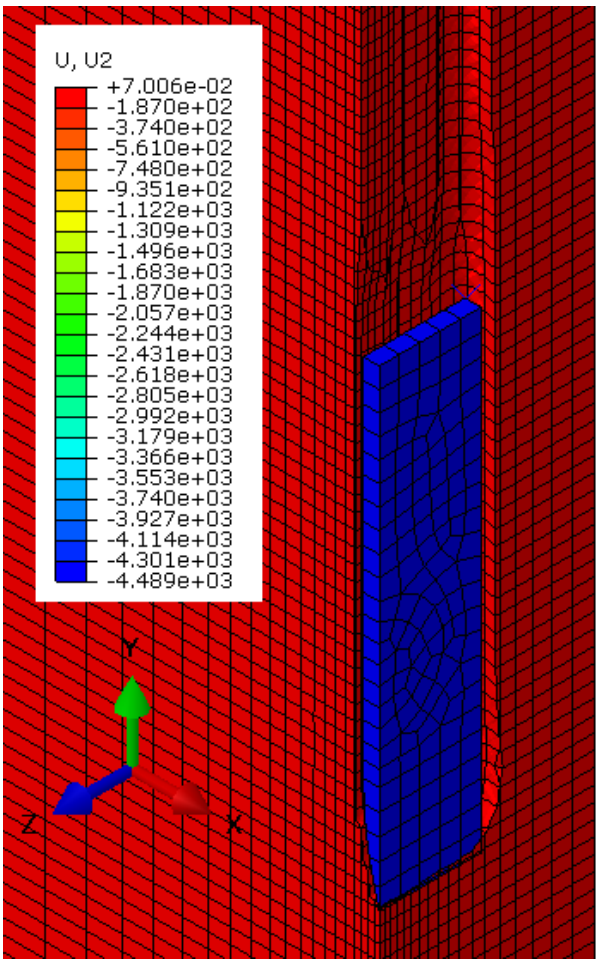


Figure 10. Contours of vertical displacement (in mm). Configuration corresponding to a depth of penetration of 4.489m.

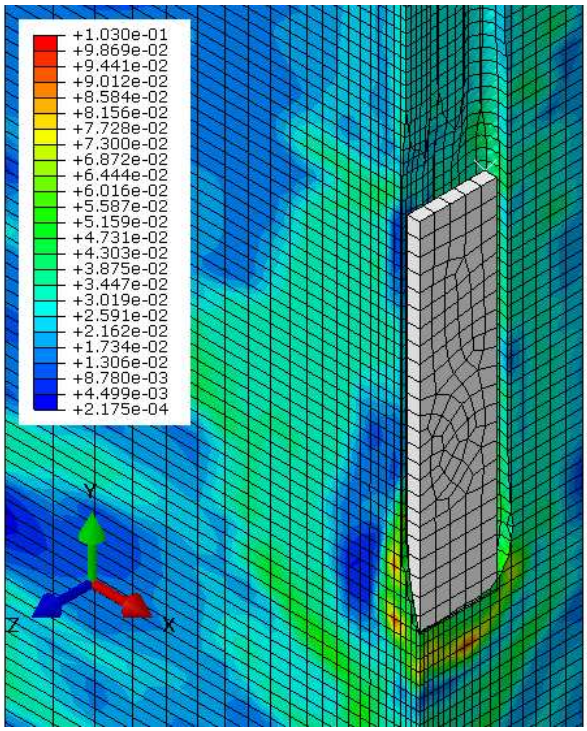


Figure 11. Contours of Mises equivalent stress at integration points (in MPa) at penetration depth of 4.489 m.

4. Conclusion

The following principal conclusions are drawn on the basis of the results obtained in the present investigation:

a) Measured DMT pressures, *po*, were found to be much higher than average numerical values computed based upon the constitutive parameters retained for the analysis. The cause is attributed to the low values of the secant Young`s moduli of the partially destructured clay.

b) Equivalent plastic strains were found to be very small, with the exception of values in close contact with the dilatometer blade.

c) Mises equivalent stresses were also found to be small in the vicinity of the dilatometer blade.

References

[1] Marchetti, S. "In situ tests by flat dilatometer", Journal of Geotechnical Engineering Division,ASCE, 106(GT3), pp. 229-231, 1980.

[2] Marchetti, S., Monaco, P., Tatani, G., and Calabrese, M. "The flat dilatometer test (DMT) in soil investigations", A report by the ISSMGE Committee TC 16. In Proceedings of the International Conference on In Situ Measurements. Soil Properties and Case Histories, Bali, May 21-24, Graduate Program, Parahyangan Catholic University, 41p, 2001.

[3] Garga, V. K., Khan, M. A. "Laboratory evaluation of K_o for overconsolidated clays", Canadian Geotechnical Journal, 28(5), pp. 650-659, 1991.

[4] Hamouche, K. K., Leroueil, S., Roy, M., Lutenegger, A. J. "In situ evaluation of K_o in eastern Canada clays", Canadian Geotechnical Journal, 32(4), pp.677-688, 1995.

[5] Lutenegger, A. J. "Cavity expansion model to estimate undrained shear strength in soft clay from dilatometer", Proceedings of the 2nd International conference on Flat Dilatometer, Washington, April 2-5, In-situ Soil Testing, pp. 319-326, 2006.

[6] Mayne, P. W. "Interrelationships of DMT and CPT readings in soft clays", Proceedings of the 2nd International Conference on Flat Dilatometer, Washington, April 2-5, In-Situ Soil Testing, pp. 220-225, 2006.

[7] Robertson, P. K. "The James K. Mitchell Lecture : Interpretation of in-situ tests. Some insights", Proceedings of Geotechnical & Geophysical Site Characterization 4, CRC Press, Boca Raton , Vol. 1 , pp. 2-24, 2009.

[8] Teh, C. I., Houslby, G. T."An analytical study of the cone penetration test", Géotechnique, 41(1):17-34, 1991.

[9] Yu, H. S. "A new procedure for obtaining design parameters from pressuremeter tests", Transactions of the Institution of Engineers, Australia, Civil Engineering, CE35(4) pp:353-359, 1983.

[10] Yu, H. S., Carter, J. P., Booker, J. R. (1993). "Analyses of the dilatometer test in undrained clay", In Predictive Soil Mechanics: Proceedings of the Wroth Memorial Symposium, Thomas Telford, London, pp. 785-795, 1993.

[11] Lacasse, S., Lunne, T. "Calibration of dilatometers correlations", Proceedings of the Ist. International Symposium on Penetration Testing. (ISOPT-1), Orlando, Balkema, Rotterdam, Vol. 1, pp. 539-548,1988.

[12] Powell, J. J. M., Uglow, I. M. . "Marchetti dilatometer testing in U.K. soils", Proceedings of the Ist International Symposium on Penetration Testing. (ISOPT-1), Orlando, Balkema, Rotterdam, Vol.1, pp. 552-562, 1988.

[13] Powell, J. J. M., Uglow, I. M. "Dilatometer testing in stiff overconsolidated clays", Proceedings of the 39th Canadian Geotechnical Conference, Ottawa, August 27-30, pp 317-326, 1986.

[14] Lutenegger, A. J., Timian, D. A. "Flat-plate penetrometer tests in marine clays", Proceedings of the 38th Canadian Geotechnical Conference, Ottawa, August 27-30, pp.301-308, 1986.

[15] Lutenegger, A .J., Blanchard, J. D. "A comparison between full displacement pressuremeter and dilatometer tests in clay", Proceedings of the 3rd International Symposium on Pressuremeters (Pressuremeters-ISP3),Oxford University, April 2-6, Thomas Telford, London, pp. 309-320, 1990.

[16] Whittle, A. J., Aubeny, C. P., Rafalovich, A., Ladd, C. C., Baligh, M. M. "Interpretation of in situ testing of cohesive soils using rational methods", Annual Report, Air Force Office of Scientific Research, Washington, 238 p.,1989.

[17] Dassault Systems. "Abaqus", 2018. Available at: https://www.3ds.com/products-services/simulia/products/abaqus.

[18] Silvestri, V. “Assessment of self-boring pressuremeter tests in sensitive clay”, Canadian Geotechnical Journal, 40(2):362-387, 2003.
[19] Hamouche, K. K. “Comportement des argiles Champlain sollicitées horizontalement”, (Behavior of Champlain clays compressed horizontally) Ph. D. Thesis, Département de Génie Civil, Université Laval, Québec, Que., Canada, 1995. (in French).
[20] Tho, K. K., Leung, C. F., Chow, Y. K., Swaddiwudhipong, S. “Eulerian finite element technique for analysis of jack-up spudcan penetration”, International Journal Geomechanics, 12(1), 64-73, 2012.
[21] Qiu, G., Henke, S., Grabe, J. “Application of coupled eulerian-lagrangian method to geotechnical problems with large deformations”, Proceedings of Simulia Customer Conference, May 18-21, London, Dassault Systems, Velizy-Villacoublay, 2009.
[22] Silvestri, V., Tabib, C. “Application of the MCC model for the estimation of undrained geotechnical parameters of clays from dilatometer tests”, Proceedings of the 3rd International Conference on the Flat Dilatometer,Rome, June 14-16, pp.431-438, 2015.